Accepted Manuscript

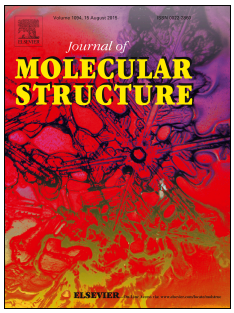

Do hydrogen bonding and noncovalent interactions stabilize nicotinamide-picric acid cocrystal supramolecular assembly?

U. Likhitha, B. Narayana, B.K. Sarojini, Anupam G. Lobo, Gopal Sharma, Surbhi Pathania, Rajni Kant

PII: S0022-2860(19)30759-8

DOI: https://doi.org/10.1016/j.molstruc.2019.06.037

Reference: MOLSTR 26679

To appear in: *Journal of Molecular Structure*

Received Date: 21 November 2018

Revised Date: 26 March 2019

Accepted Date: 11 June 2019

Please cite this article as: U. Likhitha, B. Narayana, B.K. Sarojini, A.G. Lobo, G. Sharma, S. Pathania, R. Kant, Do hydrogen bonding and noncovalent interactions stabilize nicotinamide-picric acid cocrystal supramolecular assembly?, *Journal of Molecular Structure* (2019), doi: https://doi.org/10.1016/j.molstruc.2019.06.037.

Do Hydrogen Bonding and Noncovalent Interactions Stabilize Nicotinamide-Picric Acid Cocrystal Supramolecular Assembly?

U. Likhitha[a], B. Narayana[a b]*, B. K. Sarojini[a], Anupam. G. Lobo[c], Gopal Sharma[d], Surbhi Pathania[d], Rajni Kant[d]

[a]Department of Industrial Chemistry, Mangalore University, Mangalagangothri-574199, India

[b]Department of Studies in Chemistry, Mangalore University, Mangalagangothri-574199, India

[c]School of Chemical Sciences, Mahatma Gandhi University,Kottayam -686560,India.

[d]Department of Physics, University of Jammu, Jammu Tawi - 180 006, India.

Abstract

A 1:1 stochiometric cocrystal of nicotinamide with picric acid ($C_{12}H_8N_5O_8$) has been synthesized successfully by solvent assisted grinding method and structure of the cocrystal is established by single crystal X-ray diffraction studies. The compound crystallizes in the orthorhombic space group *Pbca* with unit cell parameters: a=7.7608(11), b=14.5110 (14), c=24.751 (3) Å and Z=8. The crystal structure was solved by direct methods and refined to R=0.0723 for 1755 observed reflections. Current study has primarily focused on hydrogen bonding which is the driving force for the formation of cocrystal. Hirshfeld surfaces and fingerprint plots indicate that the structures are stabilized by O···H, N···H intermolecular interactions. In order to make a better understanding supercell model of nicotinamide-picric acid cocrystal (NICPIC) is created with crystallographic data. Based on this hydrogen bonding population, radial distribution function (RDF) and bulk properties are simulated via Molecular Dynamics (MD). Furthermore, DSC/TGA analysis indicates that the NICPIC maintains its crystallinity up to 195℃, suggesting its higher stability compared to individual components.

Keywords: Crystal structure, Direct methods, Hydrogen bonding, Hirshfeld surface, molecular dynamics.

1. Introduction

The cocrystallisation tend to enhance the physicochemical properties of APIs and great impetus is being generated in the recent past. A cocrystal alludes to two or more than two molecules combined into the same crystal lattice via intermolecular interactions such as hydrogen bonding, π-π stacking and van der Waals forces with a fixed stoichiometric ratio, which forms a special multicomponent supramolecular crystal structure [1]. Its extensive applications in pharmaceutical industry were well

documented and also attracted much attention in other fields, such as energetic materials, optical and semiconducting materials because of crystal morphology modification [2].

Many cocrystals of the compounds containing acid-amides have been synthesised by employing various cocrystal preparation strategies. Early successful experiments between nicotinamide and acids were carried out by Fábián and co-workers. Their investigation resulted that well known acid–aromatic nitrogen heterosynthon would provide sufficient driving force for cocrystallisation [3]. Examples of various cocrystals of nicotinamide with respect to those of pure acids, have also been reported by Kaup et al.
In their work they could control the formation of stoichiometric variations by adjusting the reaction mixture composition using mechanochemical process which in turn helped to manifest the mechanism of formation for the hydrogen bonded cocrystals. Interconvertibility of different stoichiometric variations by liquid assisted grinding was explored by them and it also offered qualitative rating of the relative stabilities of each cocrystal of different ratios. [4].

The presence of two nitrogen atoms of pyridine and amide in nicotinamide enables to construct reliable synthons with other molecules. It is well understood that picric acid is a known π acceptor and hence forms charge transfer complexes [5-6] [Figure 1.]. It is used in medicinal formulations in the treatment of malaria, trichinosis, smallpox and antiseptics. In view of importance of pharmaceutical cocrystals, various pharmaceutical crystals were synthesised in combination with picric acid and were reported by our group. Picrate of desipramine was synthesised by Swamy et al. [7] and its crystal structure was studied. Yathirajan et. al [8] reported the crystal structure of phthalazine-1(2H)-one in combination with picric acid having 1:1 ratio. Harrison et.al reported the crystal structure of imipraminium picrate [9]. The crystal of 2-aminopyrimidinium picrate was obtained by Narayan et.al [10] and its crystal structure was studied by them. Also, Fun et.al [11] were able to form a crystal of orphenadrinium picrate picric acid and obtained its crystal structural details. The recent approaches showed that cocrystal formation has been rationalized by considering the non-covalent interactions. Previously there have been considerable amount of studies on MD simulations of cocrystals. This included the study on thermal stability of 1,3-dinitrobenzene-2,4,6,8,10,12-hexanitro-2,4,6,8,10,12-hexaazaiso-wurtzitane cocrystal by Sun et al. The sensitivity studies of another energetic material 2,4,6,8,10,12-hexanitro-2,4,6,8,10,12-hexaazaiso-wurtzitane with trinitrotoluene studied by Guo et al. Investigation of binding energy and mechanical properties of explosive cocrystal Hexaazaisowurtzitane -Nitroguanidine with different molecular ratios was reported by Ding et al. [12-14].

Presented here is a systematic synthesis and studies on 1:1 NICPIC with its single crystal structure details and crystal packing. Focussing on simple solvent assisted grinding process it was attempted to synthesize cocrystal to seek out how pharmaceutically active small molecules like nicotinamide a part of vitamin B3 interacted with picric acid a known cocrystal former. The hydrogen bonding model is

established as a key motif in order to have an appropriate representation of NICPIC. The renowned hydrogen bonding moieties in coformers attracted to synthesize cocrystals and to further examine their hydrogen bonding patterns. To analyze this approach, MD simulation was carried out using Schrödinger's Materials Science Suite. This evidently engrossed hydrogen bonding as noncovalent interactions were most important criteria in crystal engineering which was also responsible for the stabilisation of the molecular crystal [15]. The current study also encompasses FTIR, PXRD, Hirshfeld surface analysis, RDF and bulk properties simulations which provide supportive information for the formation of stable cocrystal.

2. Experimental section

2.1. Materials and Method of preparation

The starting materials and other reagents were taken from commercial sources and were used without further purification. Mixture of nicotinamide (1.262g, 0.01M, 99.5% purity) and picric acid (2.231g, 0.01M, 99.8% purity) was ground properly using agate mortar and pestle with few drops of acetonitrile solvent. Acetonitrile (20mL) was added to this mixture and heated at 70℃. Precipita te formed was filtered and dried. It was purified by using 10 mL of ethanol-water solution (2:1) on heating to 70℃. The flakes like material obtained on cooling (4 days) was further dissolved using 15 mL of ethanol to get single crystals.

2.2 Characterization

Infrared spectra were obtained from BRUKER TENSOR II FTIR spectrometer in the spectral range 400–4000 cm^{-1} with KBr pellets. The DSC and TGA were carried out to meet the needs of cocrystal characterisation and analysis. The thermal properties of NICPIC were examined by Universal V4.5A TA Instruments SDT Q600 V20.9 Build 20 differential scanning calorimeter. The instrument was calibrated using an Indium metal. The experiments were carried out in nitrogen atmosphere with flow rate 100 $mL.min^{-1}$. Around 2-2.5 mg of each sample was loaded into an aluminium pan, and an accurately weighed blank aluminium pan was used as reference. Original samples of NICPIC and starting materials were heated from room temperature to 600℃ at a rate of 10$℃.min^{-1}$.

The cocrystal sample was crushed to reduce particle size by grinding in a mortar and pestle in order to carry out structural studies on Rigaku miniflex 600 powder X-ray diffraction with CuKα radiation (0.15406 nm). The scanning rate was 4°min^{-1} over diffraction angle of 2θ ranging from 3° to 80°. A crystal having good morp hology (0.3 x 0.2 x 0.2 mm) was chosen for three-dimensional X-ray intensity data collection. Data was collected at 293(2) K by using X'calibur CCD area-detector diffractometer equipped with graphite monochromated Mo$K\alpha$ radiation (λ = 0.71073 Å). The cell dimensions were determined by least-squares fit of angular settings of 1727 reflections in the θ range 3.83 to 28.94°**.** A total of 6636 reflections were recorded for θ ranging from 3.74 to 25.99° and out of these reflections, 2729 were found unique. 1755 reflections were treated as observed (I>2σ(I)). Data were corrected for absorption, extinction and

Lorentz-polarization factors [16]. The structure was solved by direct methods using SHELXS-97 [17]. All non-hydrogen atoms of the molecule were located in the best E-map. A full matrix least squares refinement was carried out using SHELXL-2016 [18]. All the hydrogen atoms were also located. The final refinement cycles converged to an R= 0.0723 and wR(F^2) = 0.1918 for the observed data. Residual electron densities ranged from -0.27 to 0.47e$Å^{-3}$. Atomic scattering factors were taken from International Tables for X-ray Crystallography (1992, Vol.C, Tables4.2.6.8 and 6.1.1.4). The crystallographic data are summarized in Table1. **CCDC–1857852** contains the supplementary crystallographic data for this paper. The HPLC for the NICPIC was run and chromatogram has been attached as supplementary material.

2.3. Computational methods

The 3D surface analysis and 2D finger prints speculate about the vicinity of neighbouring atoms or molecules and hence provide an important insight into crystal packing due to molecular interactions. The closeness of intermolecular contacts can be studied by Hirshfeld surfaces by measuring a normalized contact distance (d_{norm}) based on d_e, d_i and the van Der Waals radii of the atoms [19]. Where d_{norm} denotes the distance between two atoms across the surface to the atomic radii of the atoms, d_e is the distance to the closest nuclei outside the surface and d_i is the distance to the closest nuclei inside the surface from the Hirshfeld surface. These calculations were performed using CrystalExplorer17 [20]. It is a convenient computational tool that displays the unique plots for any crystal structure by colour coding short or long-range contacts [21-22]. In addition to this 3D molecular electrostatic potential is mapped over the Hirshfeld Surfaces using wave function STO-3G basis set at Hartree-Fock theory over the range of ±0.25 au.

Based on crystal packing obtained from the XRD analysis the MD simulations were carried out for NICPIC and established the equilibrium structure. The imported CIF was prepared for molecular dynamics in OPLS3 force field. The resulting structure was minimised using Desmond with the maximum iteration of 2000 and convergence threshold 1kcal.$mol^{-1}Å^{-1}$. Further, NICPIC model were optimized by MD Multistage Workflow to obtain reasonable configurations. NVT ensemble were used at temperature 300K.

MD simulation with a total simulation time of 0.100ns was performed to equilibrate the system. The total number of 7344 of frames of data was collected finally in the trajectory. After performing the MD simulation on NICPIC system it was emphasised on characterising the hydrogen bonding population and arrived at statistical analysis which speculates the number of hydrogen bonding with time frequency parameters. In this study, it was investigated the dynamics of hydrogen bonds using the time autocorrelation function, C_{HB}, defined as

$$C_{HB}(t) = < b\ (0).\ b(t) > / < b >,$$

where b(t) is 1 if a D-H···A hydrogen bond between a given set of donor, D, hydrogen, H, and acceptor, A, atoms exists at time t, and is zero otherwise [23].

RDF refers to ratio of the area density around the investigated atom and average density of the entire system, which mainly indicates the distance of a given particle from

other particles in the system. Thus, we can depict the interactions between molecules by analysing the distribution of particles in space [24]. To clarify the interactions, RDF simulation was performed in the cocrystal system. The parameters of bulk properties here include density, cohesive energy, solubility, heat of vaporisation, stress and strain. Density is a fundamental structural parameter that can be compared directly to experiment. Density (ρ) is defined as mass (*m)* per unit volume(*V),*

$$\rho = m/V$$

Density was computed for each frame over the course of the trajectory. Inspection of its convergence gives important feedback on the degree of system convergence. With the OPLS force fields, the fully equilibrated density could be computed to within 3% of experimental values.

CED implies to the energy required by 1 mole of condensates to overcome intermolecular forces and turn into gas in unit volume. This technique quantifies the magnitude of intermolecular forces in the cocrystal system, and it can also provide theoretical criterion of thermal sensitivity magnitude in a high energy system under specific conditions. Here the plot of cohesive energy is obtained with respect to different time intervals in nano seconds.

The heat of vaporization and Hildebrand solubility parameter are closely related properties. The solubility parameter is useful for estimating the miscibility of various components being considered for applications requiring multicomponent mixtures. The solubility parameter (δ) for a pure liquid is defined as

$$\delta = [(\Delta H_v - RT) / V_m]^{1/2}$$

where ΔH_v is heat of vaporization and V_m is molar volume. The heat of vaporization, ΔH_v, is measured in *kcal/mol* and is calculated from the energy of periodic unit cell minus the sum of the *N* individual molecules, E_i, averaged over the MD trajectory.

$$\Delta H_v = \{|E_{cell} - \sum_{i=1}^{N} Ei\ |\} + RT$$

The stress-strain relation is generated by subjecting a cocrystal system into arbitrary load, hence the deformation by stress and Strain i.e. relative change in the position of points within a body that has undergone deformation is quantified using MD simulations.

3. Results and discussions

3.1. FTIR analysis

As displayed in Figure 2. the pure nicotinamide showed -N-H stretching vibration at 3165cm^{-1}, strong absorption band at 1629cm^{-1} due to -C=N ring stretching vibration and the amide I and amide II absorption bands appeared at 1670cm^{-1}(-C=O) and 1598cm^{-1}(-N-H bend). These observations agree well with the IR data of nicotinamide reported in literature [25]. The absorption bands of pure picric acid appeared at 3106 cm^{-1},1540cm^{-1},1366cm^{-1} and 1256cm^{-1} which correspond to phenolic -OH stretching, aromatic -NO_2 stretching (two bands) and -NO symmetric stretching vibration respectively. These assignments are also in line with the literature values [26].

In the spectrum of synthesised NICPIC stretching modes were very much prominent, almost all characteristic bonds of nicotinamide and picric acid were evident and it is represented in Figure 2. The broad band appeared at 3090 cm^{-1} in NICPIC indicated that the -OH group of picric acid was likely involved in the intermolecular hydrogen bonds with -NH group of nicotinamide [27].

3.2. Thermogravimetric studies

The representative DSC and TGA thermographs (Figure 3.) of NICPIC and starting materials showed distinguishable features. From the DSC profile it was revealed that picric acid showed endothermic and exothermic peaks at 125.19℃ and 255.69℃ respectively. For the nicotinamide the DSC curve exhibited endothermic peak at 131.83℃ and another endothermic peak at 258.33° C. TGA curve of the NICPIC showed the continued weight loss from 200-600℃ wit h an endothermic event appeared at 195.17℃. Hence it exhibited melting point much higher than that of the starting materials. As a result of these thermal techniques for understanding the stability of cocrystal revealed that it maintained its relative crystallinity up to 195℃. This indicated that NICPIC possessed better stability than the nicotinamide and picric acid individually.

3.3. Powder and Single crystal X-ray diffraction analysis

The crystalline states for the starting materials and NICPIC have been presented in Figure 4. There were obvious differences among these powder X-ray diffraction patterns. It could be observed that original characteristic peaks of nicotinamide at 2θ=38.05° and picric acid at 2θ=8.7°, 2θ=18.02°, 2θ=23.1° and 2θ=42.4° have disappeared or declined, and few existing peaks were highly intensified at the range 6-75°. New peaks appeared at 2θ=51.2° 2θ=76.7° in NICPIC spectrum which stipulated that the obtained spectrum was different from those of the starting materials indicating the emergence of new crystalline phase. Moreover, NICPIC spectrum exhibited stronger diffraction peaks than those of two components, hence higher crystalline quality. This result emphasized that long-term stability of NICPIC would be better than those of two components [28].

An ORTEP view of the NICPIC with atomic labelling is shown in Figure 5. [29]. The geometry of the molecule was calculated using the PLATON [30] and PARST [31] software. Bond lengths and bond angles were within expected values [32]. Packing view of the molecules in the unit cell viewed down the a-axis is shown in Figure 6. Details of non-hydrogen atoms and hydrogen bonding are given in table 2-4. No significant C-H…π contacts were observed in the molecular packing of NICPIC. The crystal structure was further stabilized by π-π interactions and details of π–π interaction is given in Table 5.

3.4. Hirshfeld surface analysis

From the analysis it was revealed that the O...H (45.2%) bonding appeared to be a major contributor in the crystal packing, whereas the H···H (13.6%) , N···H (1.5%), C···H (5.6%), C···C (2.1%), C···O (12.7%), N···C (4.5%), N···N (1.4%), N···O (5.6%),

O···O (7.9%), contacts have their significant distribution to the total area of the surface as shown in Figure 7.

As illustrated in Figure 8. circular red spots visible on 3D Hirshfeld surfaces corresponded to the significant hydrogen bonding contacts such as O-H---O and N-H---O which played major role as a primary interaction seen on NICPIC. The blue region arose due to positive electrostatic potential over the Hirshfeld surface constituted hydrogen donor potential, whereas hydrogen bond acceptors are indicated by red region which extend a quantitative insight to negative electrostatic potential on the surface.

3.5. MD simulations

The resulting trajectory was analysed in Desmond-Simulation Event Analysis Panel for all the simulation work. The subsets of two compounds were selected in simulation panel and respective hydrogen bonds between these two subsets of molecules were mapped and monitored. Similarly, the resulting trajectory was imported into Desmond's RDF where the radial distance between centre of mass of nicotinamide and centre of mass of picric acid is calculated by selecting the subsets of NICPIC as done in simulation event analysis.

Intermolecular interactions(-C=O---N) were observed between -C=O and ring nitrogen of two nicotinamide molecules and a hydrogen bonding (-N-H---O) between amide -NH_2 of nicotinamide and hydroxyl group of picric acid were observed. According to the structure of nicotinamide and picric acid they could form hydrogen bond type -N-H---O. In addition, intramolecular hydrogen bonding between the two ortho nitro groups and OH group of picric acid was also evident. The short interactions like van der Waals and long interactions like H-bonding were present among the like molecules and also with coformers could be observed (Figure 9). Thus, the equilibrating structures were obtained through MD simulations and is given in Figure 10a-10f.

3.5.1. Determination of hydrogen bonding population

As a way to describe how hydrogen bonding population varies with time simulation was performed for NICPIC which resulted in varied number of hydrogen bonds with different time frequency range as depicted in the Figure 11.

It could be seen that there is a probability of 390-415 hydrogen bonds formation at time frequency 0.0ns^{-1} and those still existed when frequency reached to 0.032ns^{-1}. It showed 365-390, 415-440, 340-365 hydrogen bonds when the time frequency ranged from 0.0ns^{-1} to 0.004, 0.0025, 0.001 ns^{-1} respectively. Hence, it could be observed that there might be formation of hydrogen bonds at time 0 seconds, and still existed to time t and broke in between. The short time decay or long frequency range was seen at 0.0-0.032ns^{-1} which might be from fast motion such as intermolecular interaction in the form of hydrogen bonding. However, considerably long-time decay was observed at the range 0.004, 0.0025,0.001 and 0.0005ns^{-1}.

Another point to consider is that the nature of hydrogen bonding also depends upon its stretching frequency. Nakamoto et al. have obtained the measurements of hydrogenic stretching frequencies of a number of hydrogen bonded compounds. Their

work highlighted the behaviour of hydrogen bonds which portrayed straight, bent and bifurcated bonds would show high and low frequency deviations respectively. Most intermolecular hydrogen bonds were found to be straight, but a large number of intramolecular hydrogen bonds must be bent if normal bond angles were to be preserved [33].

In comparison with the graph obtained from simulation the number of hydrogen bonds formed at different time frequencies were different. This might be due to the formation of straight, bent and bifurcated bonds which changes according to its stretching frequencies. So, complementing evidence of straight type hydrogen bonds might be formed in large numbers denoting intermolecular interaction in NICPIC. Hence, these interactions might be the guiding force for stabilizing cocrystal formation.

3.5.2. RDF simulation

A sharp peak in the RDF spectrum (Figure 12.) represents particularly favoured distance of separation of neighbouring particles to a given particles. Thus, atomic structure of the simulated system could be studied by RDF analysis. The well-defined molecular structure of the NICPIC revealed that there was a broad diffraction peak appearing in the range of 6.2–8.4 Å with a g(r) having value of about 1.15. This meant that it was only once likely that two molecules could be found at this separation [34]. The radial distribution function then falls and passes through a minimum value at around distance 9 Å. The chances of finding two molecules with this separation are less. Due to the varying lengths of hydrogen bond and strong van der Waals forces ranging from 5.5-8.5 Å it could be deduced that hydrogen bonds and strong van der Waals forces existed in NICPIC model and they might have a strong impact on the formation of the cocrystal.

3.5.3. Bulk properties

The average value of density obtained for the simulated structure is 1.16 gcm^{-3}. It does not show any typical fluctuations as the time ranges to 0.0-0.10ns as shown in Figure 13., which indicated that density of NICPIC formed does not vary with time hence it is stable.

Simulation results for solubility and cohesive energy in which the average solubility and cohesive energy of the NICPIC is 31.99 $MPa^{1/2}$ and 25.66 $kcalmol^{-1}$ respectively, did not show any variations with increase in time. Since the cohesive energy is the sum of the intermolecular forces that hold the material intact [35], it could be said that hydrogen bonding and van der Waals forces have great impact on the stability of the cocrystal. It could also be responsible for no change in cohesive energy in the graph recorded. The heat of vaporisation was found to be 26.26 $kcal.mol^{-1}$ and it remained constant with time.

The stress-strain curve of the NICPIC model is represented in Figure 14., in which deformation response varied considerably. In the early portion of the curve it was observed that NICPIC fails to withstand a tensile stress and shows a drop from 1.8 GPa to 1.1 GPa. This was probably because of weak forces like hydrogen bonding and van der Waals between partners which could play a major role to form cocrystal

architecture. These non-covalent bonds were broken down and two molecules were separated. Further, these molecules experienced the stress separately and respective deformation was observed in the plot.

4. Conclusions

A novel 1:1 NICPIC was synthesized, its X-ray quality single crystals were obtained and characterized by single crystal XRD, FTIR, PXRD and TGA/DSC. The obtained melting point of NICPIC was higher than that of the pure components. Its supramolecular architecture was stabilized by hydrogen bonding. Both the nicotinamide and picric acid contribute towards hydrogen bonding by C-H--O, N-H--O interactions. It was evident from the Hirshfeld surface analysis that there exist 45.2% of -O--H bonding which was the major contributor in the crystal packing of NICPIC. It was also possible to recognize the hydrogen bonding motifs by RDF and bulk properties simulation. Hence the results presented herein are step towards the better understanding of hydrogen bonding through cocrystallisation which results in supramolecular assembly.

5. List of abbreviations

The following are the list of abbreviations used in this paper:

1. CIF — Crystallographic Information File
2. CCDC— The Cambridge Crystallographic Data Centre

Supplementary material

CCDC–1857852 contains the supplementary crystallographic data for this paper. These data can be obtained free of charge from The Cambridge Crystallographic Data Centre via www.ccdc.cam.ac.uk/data_request/cif.

Acknowledgments

We thank DST-PURSE Lab, Mangalore University for Thermal analysis data and Department of Pharmaceutical Chemistry, NGSMIPS, Karnataka for spectral analysis. BN thanks UGC for financial assistance through BSR one-time grant (SR/S/Z/-23/2010/32) for the purchase of chemicals. RK thanks Department of Science and Technology, New Delhi for financial support under research Project No. EMR/2014/000467. UL is grateful to Mangalore University for research facilities.

References

[1] V. Vinesha, M. Sevukarajan, R. Rajalakshmi, G.T. Chowdary, K. Haritha, S. Vidyanikethan, C. Dt, A. Pradesh, enhancement of solubility of tadalafil by cocrystal approach bioavailability and ultimately upon the solubility of drug ingredient (API) and a co former which may / may not have should contain either hydrogen donor or accepting groups Crystal form I Cry, 4 (2013) 218–223. doi:10.7897/2230-8407.04444.

[2] P. yuan Chen, L. Zhang, S. guan Zhu, G. bin Cheng, Theoretical study ofBTF/TNA cocrystal: Effects of hydrostatic pressure and temperature, Def. Technol. 11 (2015) 132–139. doi:10.1016/j.dt.2015.01.003.

[3] L. Fábián, N. Hamill, K.S. Eccles, H.A. Moynihan, A.R. Maguire, L. McCausland, S.E. Lawrence, Cocrystals of fenamic acids with nicotinamide, Cryst. Growth Des. 11 (2011) 3522–3528. doi:10.1021/cg200429j.

[4] G.Kaupp, Mechanochemistry: The varied applications of mechanical bond-breaking, CrystEngComm. 11 (2009) 388–403. doi:10.1039/b810822f.

[5] T. Misiaszek, Z. Czyznikowska, The nature of interactions in nicotinamide crystal,J. Mol. Graph. Model. 51 (2014) 73–78 doi:10.1016/j.jmgm.2014.04.007.

[6] P. Vishnoi, S. Sen, G.N. Patwari, R. Murugavel, Charge transfer aided selective sensing and capture of picric acid by triphenylbenzenes, New J. Chem. 39 (2015) 886–892. doi:10.1039/c4nj01093k.

[7] M.T. Swamy, M.A. Ashok, H.S. Yathirajan, B. Narayana, M. Bolte, Desipraminium picrate, Acta Crystallogr. Sect. E Struct. Reports Online. 63 (2007). doi:10.1107/S1600536807062393.

[8] H.S. Yathirajan, B. Narayana, M.T. Swamy, B.K. Sarojini, M. Bolte, Phthalazin-1(2H)-one-picric acid (1/1), Acta Crystallogr. Sect. E Struct. Reports Online. 64 (2008). doi:10.1107/S1600536807063362.

[9] W.T.A. Harrison, S. Bindya, M.A. Ashok, H.S. Yathirajan, B. Narayana, Imipraminium picrate, Acta Crystallogr. Sect. E Struct. Reports Online. 63 (2007) 1188–1195. doi:10.1107/S1600536807026050.

[10] B. Narayana, B.K. Sarojini, K. Prakash Kamath, H.S. Yathirajan, M. Bolte, 2-Aminopyrimidinium picrate,ActaCrystallogr. Sect. E Struct. Reports Online. 64 (2008). doi:10.1107/S1600536807062599.

[11] H.K. Fun, M. Hemamalini, B.P. Siddaraju, H.S. Yathirajan, B. Narayana, Orphenadrinium picrate picric acid, Acta Crystallogr. Sect. E Struct. Reports Online. 66 (2010). doi:10.1107/S1600536810006379.

[12] T. SUN, J.J. Xiao, G. Ji, F. Zhao, H. Xiao, Molecular Dynamics Simulation Studies of the CL-20/DNB Co-crystal, Cent. Eur. J. Energ. Mater. 13 (2016) 677–693. doi:10.22211/cejem/65015.

[13] D. Guo, Q. An, W.A. Goddard, S. V. Zybin, F. Huang, Compressive shear reactive molecular dynamics studies indicating that cocrystals of TNT/CL-20 decrease sensitivity, J. Phys. Chem. C. 118 (2014) 30202–30208. doi:10.1021/jp5093527.

[14] X. Ding, R. Gou, F. Ren, F. Liu, S. Zhang, H. Gao, Molecular Dynamics Simulation and Density Functional Theory Insight into the Cocrystal Explosive of Hexaazaisowurtzitane / Nitroguanidine, (2015). doi:10.1002/qua.25027.

[15] T. Misiaszek, Z. Czyznikowska, The nature of interactions in nicotinamide crystal, J. Mol. Graph. Model. 51 (2014) 73–78. doi:10.1016/j.jmgm.2014.04.007.

[16] Oxford Diffraction, Crys Alis PRO. Oxford Diffraction Ltd (2010),Yarnton Oxfordshire, England.

[17] G.M. Sheldrick, A short history of SHELX, Acta Crystallogr. Sect. A Found. Crystallogr. 64 (2008) 112–122. doi:10.1107/S0108767307043930.

[18] G.M. Sheldrick, Crystal structure refinement with SHELXL, Acta Crystallogr. Sect. C Struct. Chem. 71 (2015) 3–8. doi:10.1107/S2053229614024218.

[19] J.J. McKinnon, A.S. Mitchell, M.A. Spackman, Hirshfeld surfaces: A new tool for visualising and exploring molecular crystals, Chem. - A Eur. J. 4 (1998) 2136–2141. doi:10.1002/(SICI)1521-3765(19981102)4:11<2136::AID-CHEM2136>3.0.CO;2-G.

[20] M. J. Turner, J. J. McKinnon, S. K. Wolff, D. J. Grimwood, P. R. Spackman, D. Jayatilaka and M. A. Spackman, CrystalExplorer17 (2017). University of Western Australia.

[21] Y.H. Ma, S.W. Ge, W. Wang, B.W. Sun, Studies on the synthesis, structural characterization, Hirshfeld analysis and stability of apovincamine (API) and its co-crystal (terephthalic acid: Apovincamine = 1:2), J. Mol. Struct. 1097 (2015) 87–97. doi:10.1016/j.molstruc.2015.05.014.

[22] V. V. Salian, B. Narayana, B.K. Sarojini, M.S. Kumar, G.S. Nagananda, K. Byrappa, A.K. Kudva, Spectroscopic, single crystal X-ray, Hirshfeld, in vitro and in silico biological evaluation of a new series of potent thiazole nucleus integrated with pyrazoline scaffolds, Spectrochim. Acta - Part A Mol. Biomol. Spectrosc. 174 (2017) 254–271. doi:10.1016/j.saa.2016.11.046.

[23] A. Lerbret, F. Affouard, Molecular Packing, Hydrogen Bonding, and Fast Dynamics in Lysozyme/Trehalose/Glycerol and Trehalose/Glycerol Glasses at Low Hydration, J. Phys. Chem. B. 121 (2017) 9437–9451. doi:10.1021/acs.jpcb.7b07082.

[24] S. Xiong, S. Chen, S. Jin, Molecular dynamic simulations on TKX-50/RDX cocrystal, J. Mol. Graph.

Model. 74 (2017) 171–176. doi:10.1016/j.jmgm.2017.03.006.
[25] S. Ramalingam, S. Periandy, M. Govindarajan, S. Mohan, FT-IR and FT-Raman vibrational spectra and molecular structure investigation of Nicotinamide: A combined experimental and theoretical study, Spectrochim. Acta - Part A Mol. Biomol. Spectrosc. 75 (2010) 1552–1558. doi:10.1016/j.saa.2010.02.015.
[26] A. Manuscript, www.rsc.org/analyst, (n.d.)
[27] M. Liu, C. Hong, Y. Yao, H. Shen, G. Ji, G. Li, Y. Xie, Development of a pharmaceutical cocrystal with solution crystallization technology: Preparation, characterization, and evaluation of myricetin-proline cocrystals, Eur. J. Pharm. Biopharm. 107 (2016) 151–159. doi:10.1016/j.ejpb.2016.07.008.
[28] N.H. Chun, I.C. Wang, M.J. Lee, Y.T. Jung, S. Lee, W.S. Kim, G.J. Choi,Characteristics of indomethacin-saccharin (IMC-SAC) co-crystals prepared by an anti-solvent crystallization process, Eur. J. Pharm. Biopharm. 85 (2013) 854–861.
[29] L.J. Farrugia, WinGX and ORTEP for Windows: An update, J. Appl. Crystallogr. 45 (2012) 849–854. doi:10.1107/S0021889812029111.
[30] A.L. Spek, Structure validation in chemical crystallography, Acta Crystallogr. Sect. D Biol. Crystallogr. 65 (2009) 148–155. doi:10.1107/S090744490804362X.
[31] M. Nardelli, computer programme abstarct, J Appl. Cryst. (1995)*28*, 659.
[32] F.H. Allen, O. Kennard, D.G. Watson, L. Brammer, A.G. Orpen, R. Taylor, Tables of Bond Lengths determined by X-Ray and Neutron Diffraction, J. Chem. Soc. Perkin Trans. 2. (1987) 1–19. doi:10.1039/p298700000s1.
[33] K. Nakamoto, M. Margoshes, R.E. Rundle, Stretching Frequencies as a Function of Distances in Hydrogen Bonds, J. Am. Chem. Soc. 77 (1955) 6480–6486. doi:10.1021/ja01629a013.
[34] A. Hsu, Molecular Dynamics Simulations of Hydrophobic Solutes in Liquid Water, (2007) 1–61.
[35] S.R. Fukte, M.P. Wagh, S. Rawat, Coformer selection: An important tool in cocrystal formation, Int. J. Pharm. Pharm. Sci. 6 (2014) 9–14.

Do Hydrogen Bonding and Noncovalent Interactions Stabilize Nicotinamide-Picric Acid Cocrystal Supramolecular Assembly?

U. Likhitha[a], B. Narayana[a b]*, B. K. Sarojini[a], Anupam. G. Lobo[c], Gopal Sharma[d], Surbhi Pathania[d], Rajni Kant[d]

[a]Department of Industrial Chemistry, Mangalore University, Mangalagangothri-574199, India

[b]Department of Studies in Chemistry, Mangalore University, Mangalagangothri-574199, India

[c]School of Chemical Sciences, Mahatma Gandhi University, Kottayam -686560, India.

[d]Department of Physics, University of Jammu, Jammu Tawi - 180 006, India.

Table 1: Crystal and experimental data

CCDC No.	**1857852**
Crystal description	Block
Crystal colour	Colourless
Crystal size	0.30 x 0.20 x 0.20 mm
Empirical formula	$C_{12}H_8N_5O_8$
Formula weight	350.23
Radiation, Wavelength	Mo Kα, 0.71073 Å
Unit cell dimensions	a = 7.7608 (11), b =14.5110 (14), c = 24.751(3) Å
Crystal system	Orthorhombic
Space group	*Pbca*
Unit cell volume	2787.3(6)
No. of molecules per unit cell, Z	8
Temperature	293(2)
Absorption coefficient	0.144 mm^{-1}
F (000)	1432
Scan mode	ω scan
θ range for entire data collection	3.83 <θ< 28.94 º
Range of indices	h= -6 to 9, k= -17 to 13, l= -30 to 24
Reflections collected / unique	6636 / 2729
Absorption correction	Multi-scan i. CrysAlis RED
Reflections observed (I > 2σ(I))	1755
R_{int}	0.0427
R_{sigma}	0.0545
Structure determination	Direct methods
Refinement	Full-matrix least-squares on F^2
No. of parameters refined	259

No. of Restraints	0
Final R	0.0723
wR(F^2)	0.1918
Weight	$1/ [\sigma^2(F_o^2) +(0.1117 P)^2+ 1.7781P]$ where $P= [F_o^2 +2F_c^2] / 3$
Goodness-of-fit	1.036
(Δ /σ) max	0.002
Final residual electron density	$-0.27< \Delta\rho < 0.47$ eÅ^{-3}
Measurement	X'calibur system – Oxford diffraction make, U.K.
Software for structure solution	SHELXL-97 (Sheldrick, 2008)
Software for refinement	SHELXL-2016/6 (Sheldrick, 2016)
Software for molecular plotting	ORTEP-3 (Farrugia, 2012) PLATON (Spek, 2009)

Table 2: Bond lengths (Å) and bond angles (°) for non-hydrogen atoms (e.s.d.'s is given in parentheses)

Bond Lengths (Å)		Bond Lengths (Å)	
C1-C2	1.382 (4)	C12-C11	1.380 (5)
C3-C2	1.387 (5)	N1-C1	1.342 (4)
C3-C4	1.392 (5)	N1-C5	1.330 (5)
C5-C4	1.368 (5)	N3-O2	1.218 (5)
C6-C2	1.506 (4)	N3-O3	1.217 (4)
C6-N2	1.306 (5)	N4-O4	1.194 (4)
C7-C8	1.449 (5)	N5-C11	1.449 (5)
C7-N3	1.454 (5)	N5-O6	1.230 (4)
C9-C8	1.452 (5)	O1-C6	1.241 (4)
C9-C10	1.360 (5)	O5-N4	1.217 (4)
C9-N4	1.464 (5)	O7-N5	1.212 (4)
C11-C10	1.387 (5)	O8-C8	1.242 (4)
C12-C7	1.368 (5)		
Bond Angles (°)		Bond Angles (°)	
N1-C1-C2	119.2 (3)	C10-C9-C8	123.8 (3)
C1-C2-C3	118.6 (3)	C10-C9-N4	116.5 (3)
C1-C2-C6	123.3 (3)	C9-C10-C11	119.6 (3)
C3-C2-C6	118.1 (3)	C10-C11-N5	118.9 (3)
C2-C3-C4	120.5 (3)	C12-C11-C10	121.2 (3)
C5-C4-C3	118.2 (4)	C12-C11-N5	119.9 (3)
N1-C5-C4	120.4 (3)	C7-C12-C11	119.1 (4)
N2-C6-C2	118.8 (3)	C5-N1-C1	123.0 (3)
O1-C6-C2	118.1 (3)	O2-N3-C7	118.7 (3)
O1-C6-N2	123.2 (3)	O3-N3-C7	120.7 (3)
C8-C7-N3	119.2 (3)	O3-N3-O2	120.6 (3)
C12-C7-C8	124.2 (3)	O4-N4-C9	120.2 (3)
C12-C7-N3	116.5 (3)	O4-N4-O5	122.3 (3)
C7-C8-C9	112.1 (3)	O5-N4-C9	117.5 (3)
O8-C8-C7	123.3 (3)	O6-N5-C11	118.5 (3)
O8-C8-C9	124.6 (3)	O7-N5-C11	118.8 (3)
C8-C9-N4	119.7 (3)	O7-N5-O6	122.6 (3)

Table 3: Torsion angles (°) for non-hydrogen atoms (e.s.d.'s is given in parentheses)

Torsion Angles (°)		Torsion Angles (°)	
N1-C1-C2-C3	-2.2 (6)	N4-C9-C8-C7	179.1 (3)
N1-C1-C2-C6	179.0 (3)	N4-C9-C8-O8	0.5 (6)
C4-C3-C2-C1	1.3 (6)	C8-C9-C10-C11	0.7 (6)
C4-C3-C2-C6	-179.8 (4)	N4-C9-C10-C11	-179.5 (3)
C2-C3-C4C5	-0.2 (7)	C8-C9-N4-O4	22.9 (5)
N1-C5-C4-C3	-0.1 (7)	C8-C9-N4-O5	-157.3 (3)
N2-C6-C2-C1	5.1 (6)	C10-C9-N4-O4	-156.9 (4)
N2-C6-C2-C3	-173.8 (4)	C10-C9-N4-O5	22.9 (5)
O1-C6-C2-C1	-174.8 (4)	C12-C11-C10-C9	-0.4 (6)
O1-C6-C2-C3	6.4 (6)	N5-C11-C10-C9	179.8 (3)
C12-C7-C8-C9	1.4 (5)	C11-C12-C7-C8	-1.2 (6)
C12-C7-C8-O8	179.9 (4)	C11-C12-C7-N3	-179.2 (3)
N3-C7-C8-C9	179.3 (3)	C7-C12-C11-C10	0.6 (6)
N3-C7-C8-O8	-2.1 (6)	C7-C12-C11-N5	-179.6 (3)
C8-C7-N3-O2	-161.5 (4)	C5-N1-C1-C2	2.1 (6)
C8-C7-N3-O3	19.7 (5)	C1-N1-C5-C4	-0.9 (7)
C12-C7-N3O2	16.6 (5)	O6-N5-C11-C10	-3.2 (5)
C12-C7-N3-O3	-162.2 (4)	O6-N5-C11-C12	177.0 (4)
C10-C9-C8-C7	-1.1 (5)	O7-N5-C11-C10	177.6 (4)
C10-C9-C8-O8	-179.7 (4)	O7-N5-C11-C12	-2.2 (6)

Table 4: Hydrogen bonding geometry (e.s.d`s in parentheses)

D–H…A	D–H(Å)	H…A(Å)	D…A(Å)	D–H…A(^{o})
C3-H3…O1	0.93	2.43	2.7494	100
C12-H12…O7	0.79	2.45	2.7256	102
C4-H4…O5^{i}	0.94	2.55	3.4941	175
C5-H5…O6^{ii}	1.07	2.54	3.5099	151
N2-H21…O3^{iii}	0.93	2.31	3.2041	161
N2-H22…O4^{iv}	0.96	2.43	2.8792	108
N2-H22…O8 ^{iv}	0.96	1.82	2.7716	171
C1-H1…O3 ^{iv}	0.97	2.52	3.2669	134
C1-H1…O8 ^{iv}	0.97	2.16	3.0752	156

Symmetry code:
(i) x+1/2, y, -z+1/2 (ii) 1-x, y, -z+1/2 (iii) -x+1, y-1/2, -z+1/2(iv) x+1/2, y, -z+1/2

Table 5:Geometry of π–π interactions*

CgI…CgJ	CgI…CgJ(Å)	CgI…P(Å)	α(^{o})	β(^{o})	Δ(Å)
Cg1…Cg1	3.8806	3.423	4.15	28.20	1.827

Symmetry code: x-1/2, y, -z+1/2

Where Cg1 represents the center of gravity of phenyl ring (C7-C12).

Table 6: Bulk properties

	Volume Å^3	Density gcm^{-3}	Cohesive Energy kcalmol^{-1}	Solubility MPa$^{1/2}$	Solubility vdW MPa$^{1/2}$	Solubility Ele MPa$^{1/2}$	Heat of Vap. kcalmol^{-1}
Average	75261.27	1.67	25.66	31.99	24.71	20.32	26.26
Stdev.	0.000	0.000	0.093	0.058	0.064	0.097	0.093

Do Hydrogen Bonding and Noncovalent Interactions Stabilize Nicotinamide-Picric Acid Cocrystal Supramolecular Assembly?

U. Likhitha[a], B. Narayana[a b]*, B. K. Sarojini[a], Anupam. G. Lobo[c], Gopal Sharma[d], Surbhi Pathania[d], Rajni Kant[d]

[a]Department of Industrial Chemistry, Mangalore University, Mangalagangothri-574199, India

[b]Department of Studies in Chemistry, Mangalore University, Mangalagangothri-574199, India

[c]School of Chemical Sciences, Mahatma Gandhi University, Kottayam -686560, India.

[d]Department of Physics, University of Jammu, Jammu Tawi - 180 006, India.

Graphical abstract

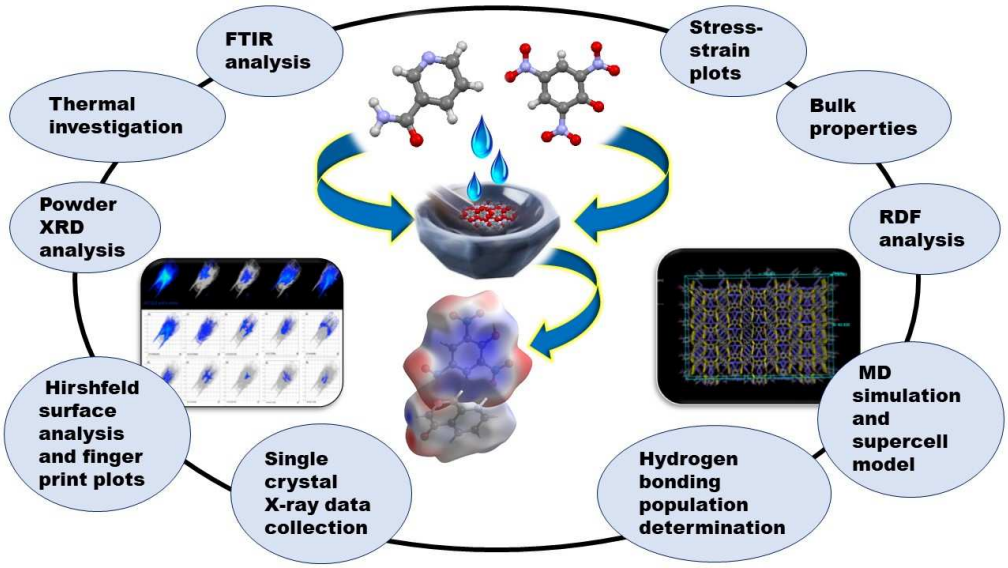

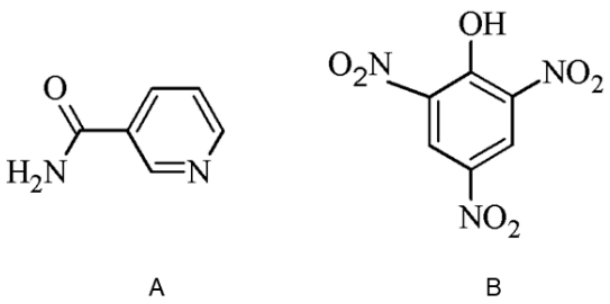

A B

Figure 1. Chemical structures of nicotinamide (A) and picric acid (B)

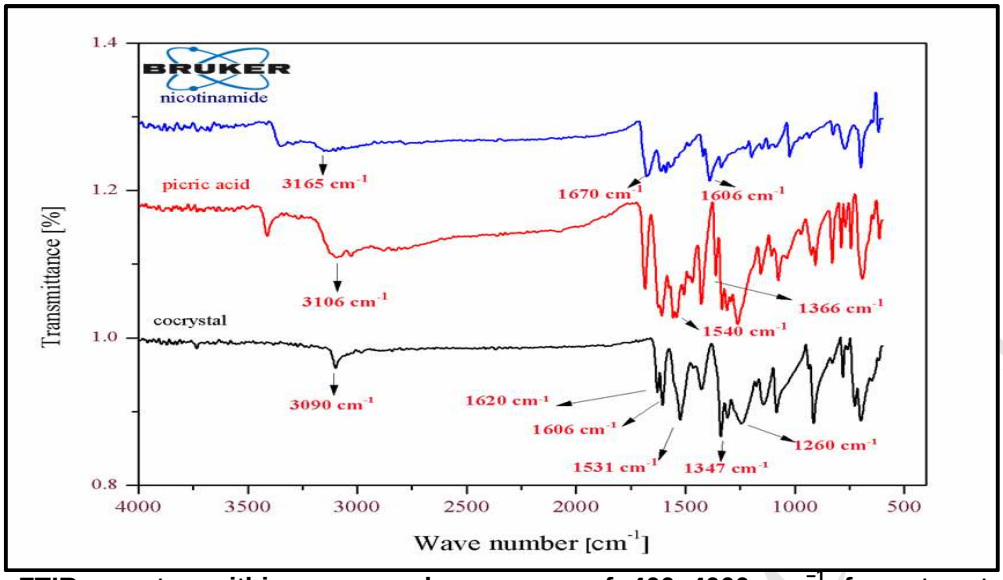

Figure 2: FTIR spectra within wavenumber ranges of 400−4000 cm^{-1} from top to bottom: nicotinamide, picric acid and NICPIC respectively.

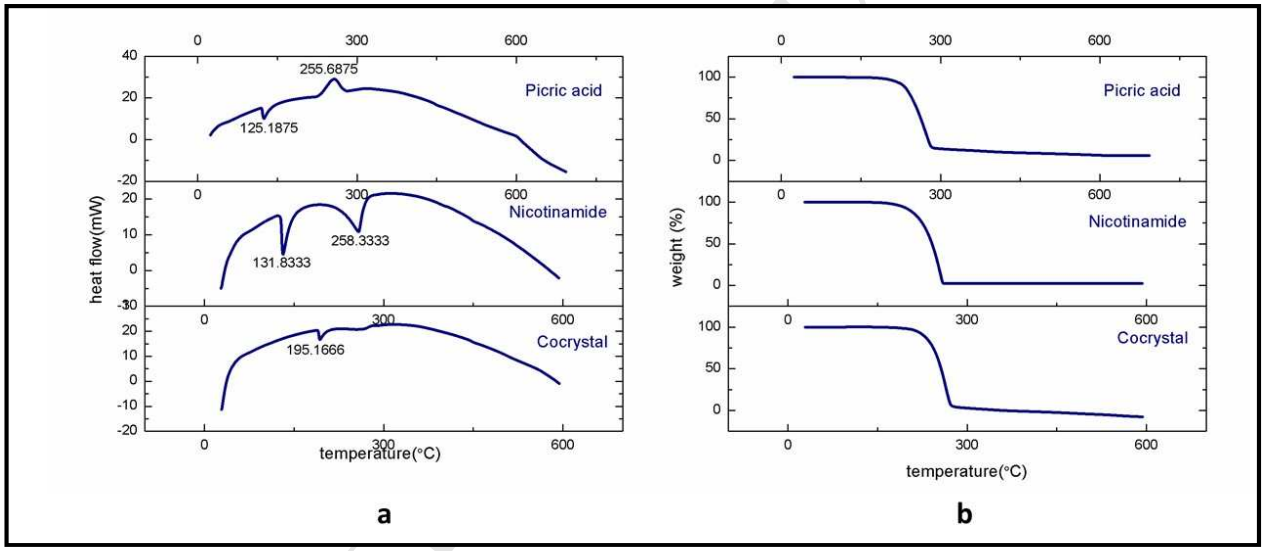

Figure 3: DSC (a) and TGA (b) results of pure picric acid, nicotinamide and NICPIC

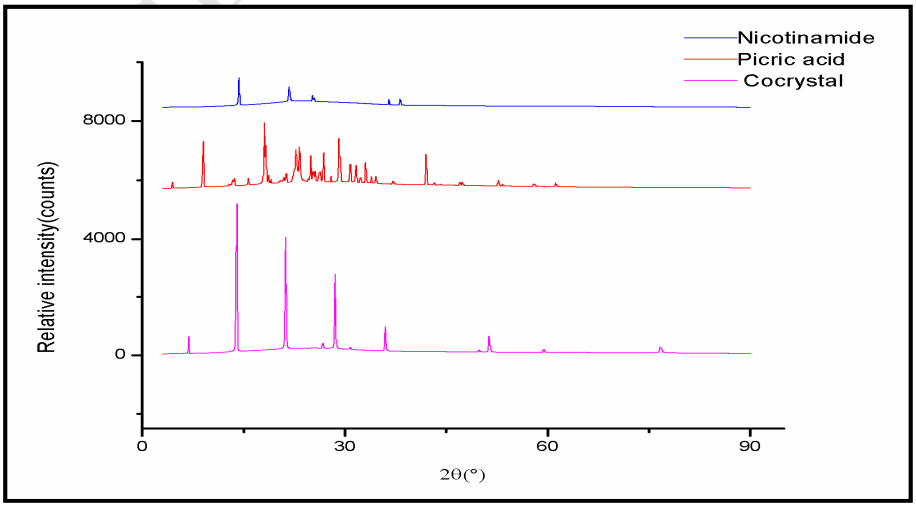

Figure 4: PXRD patterns of nicotinamide, picric acid and NICPIC

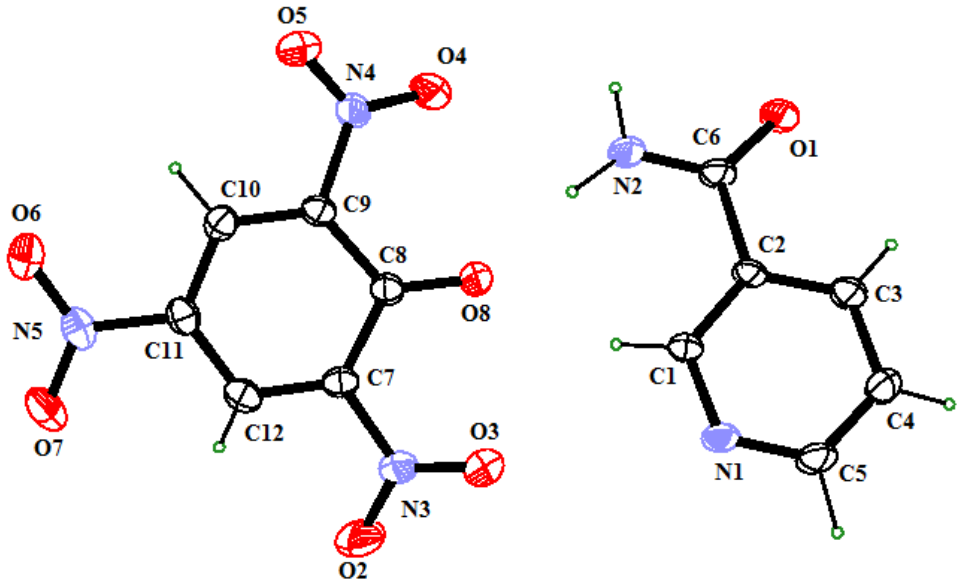

Figure 5: Showing ORTEP view of the molecule with displacement ellipsoids drawn at the 40% probability level. Hydrogen atoms are shown as small spheres of arbitrary radii

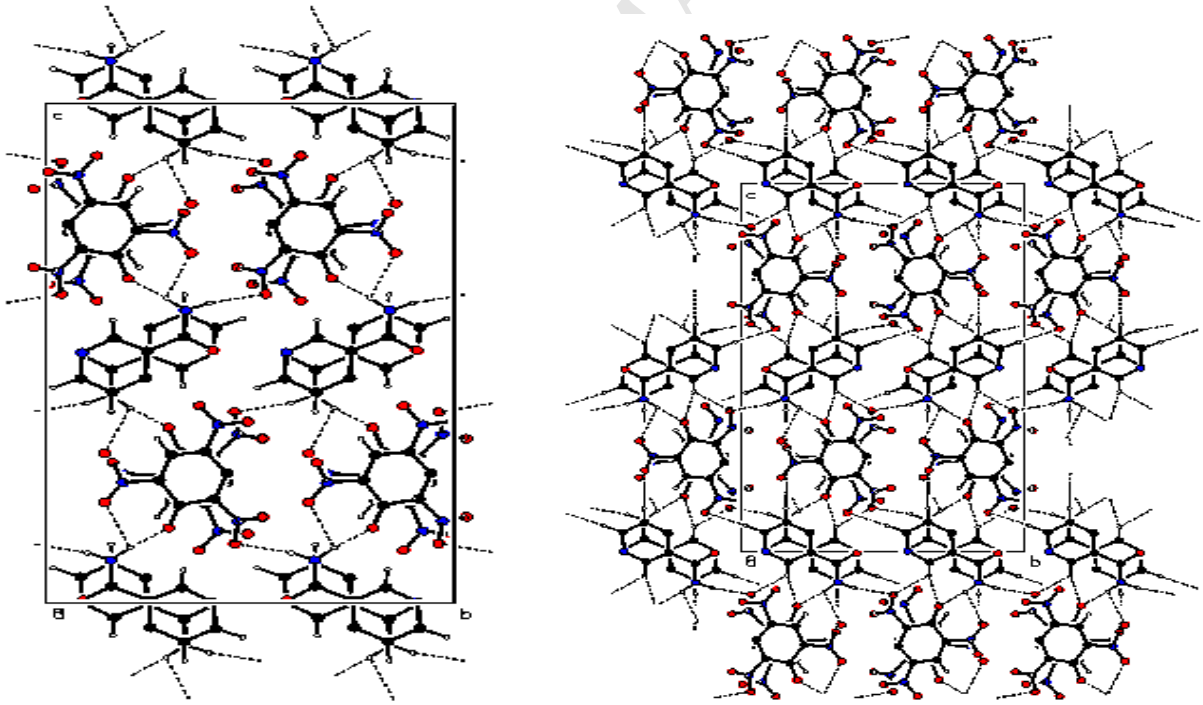

Figure 6: Packing view of the molecule viewed down the a-axis

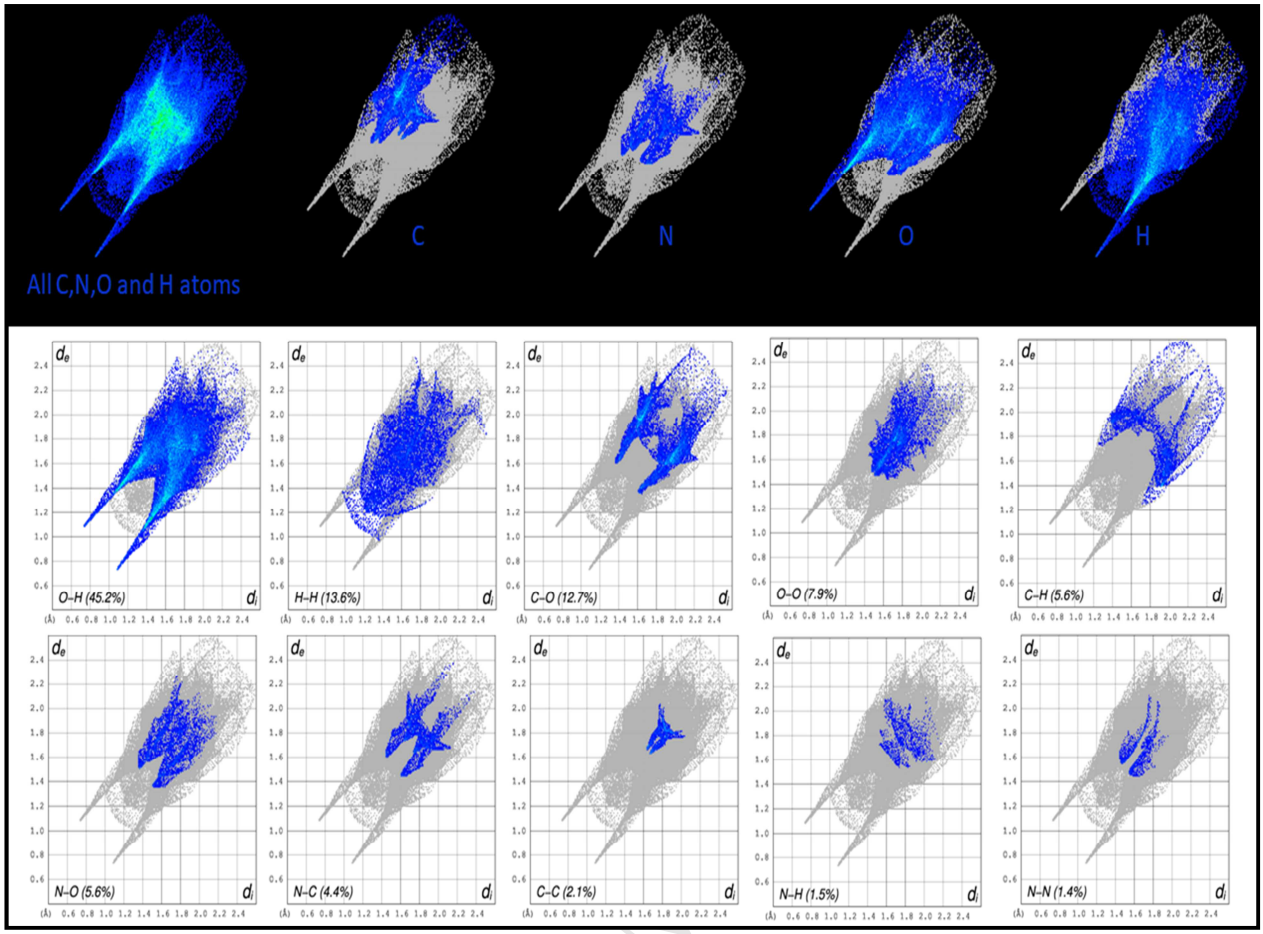

Figure 7: Fingerprint plots of the NICPIC showing molecular interactions. Here d_i is the closest internal distance and d_e is the closest external contacts from a given point on the Hirshfeld surface.

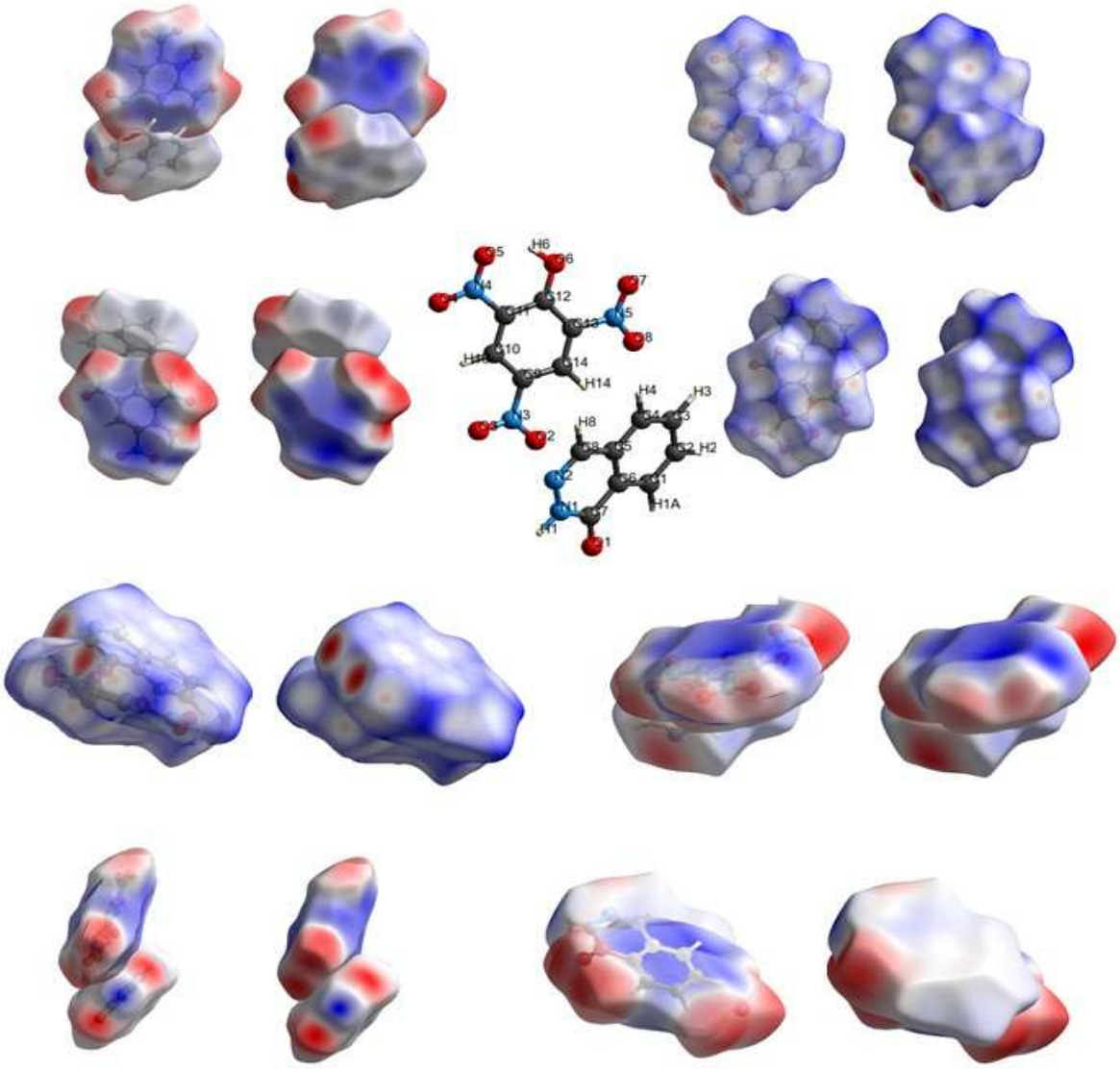

Figure 8: 3-D d_{norm} surfaces mapping with different orientations

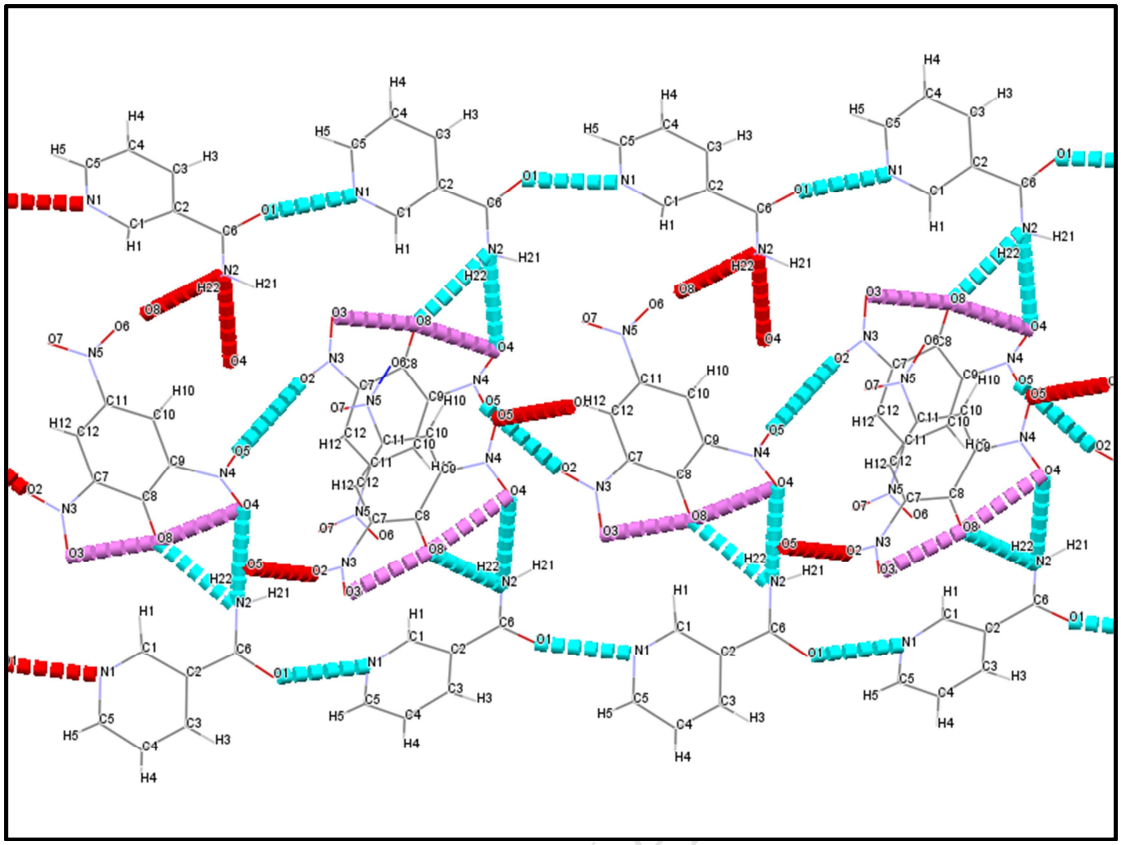

Figure 9: A view of supramolecular chain showing the hydrogen bonding in NICPIC (blue colour represents intermolecular interactions, violet colour represents intramolecular interactions and red represents expandable network in NICPIC)

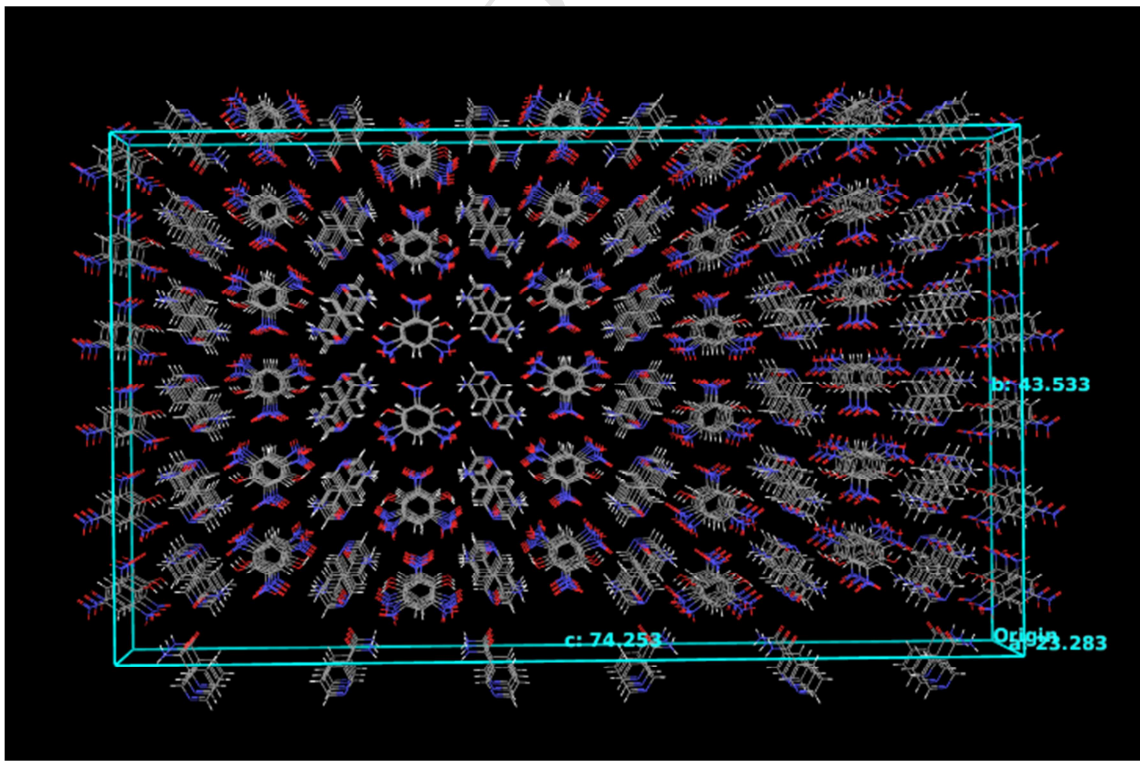

(10 a)

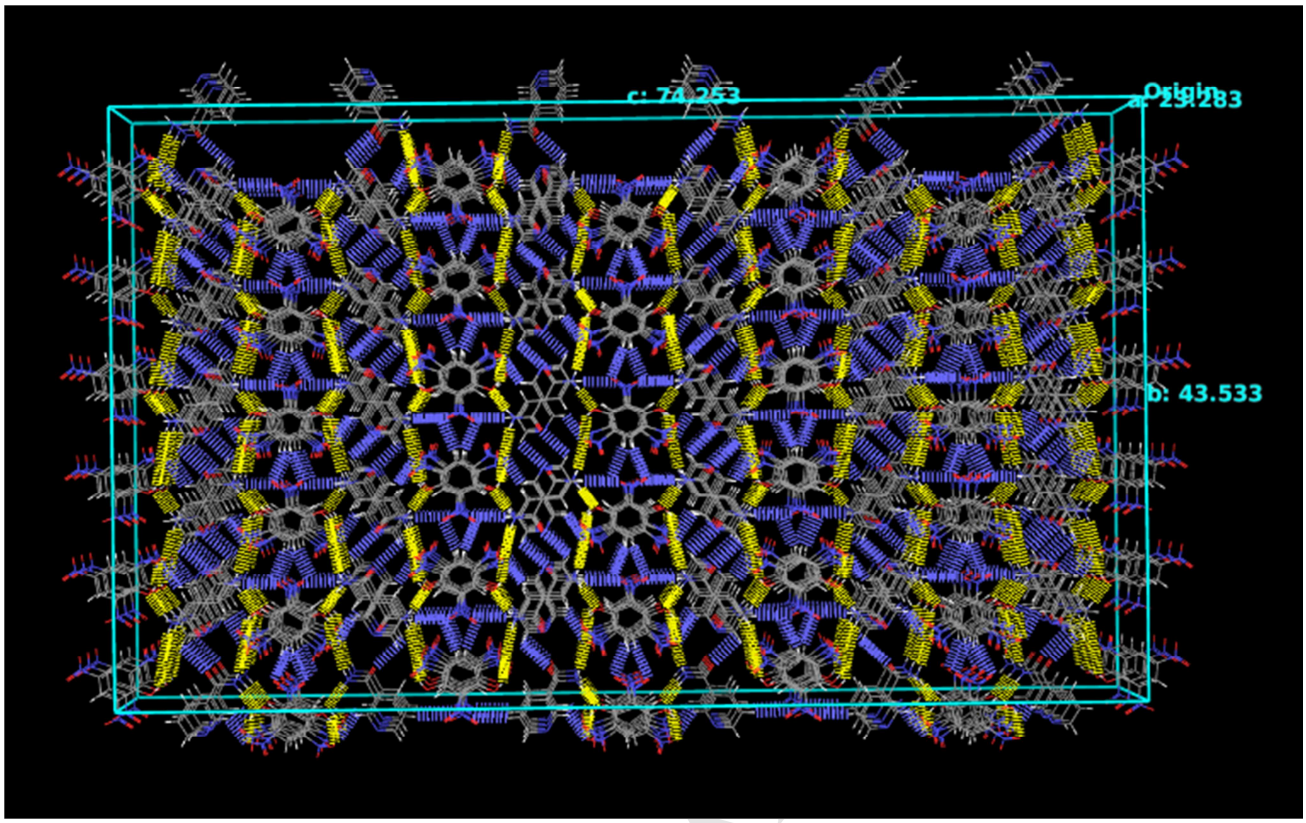

(10 b)

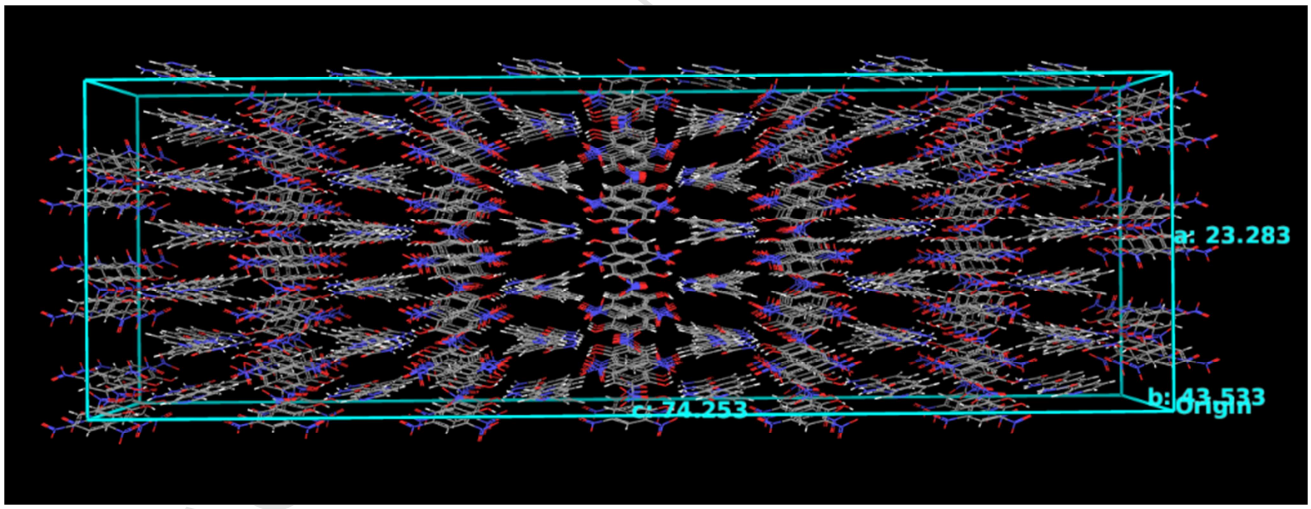

(10 c)

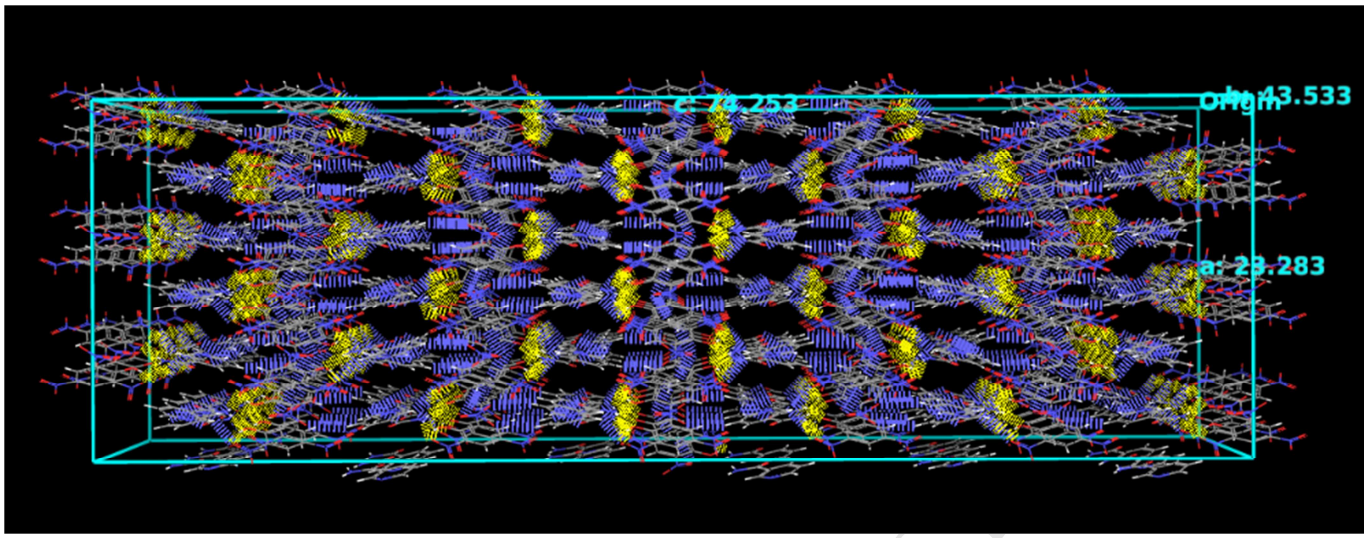

(10 d)

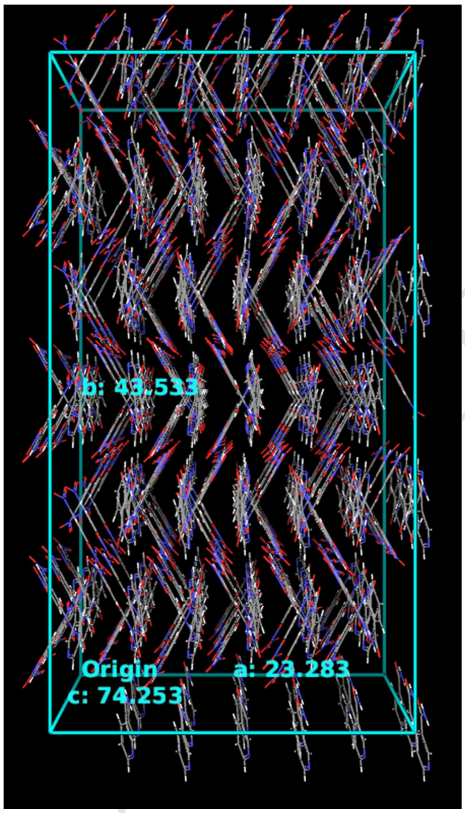

(10 e)

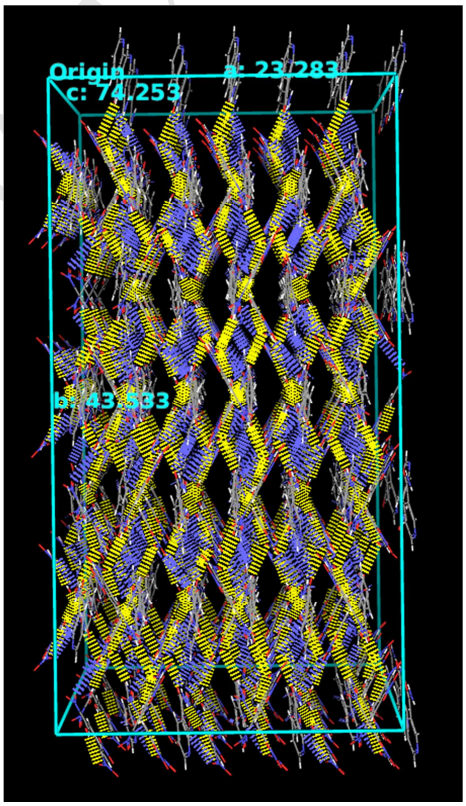

(10 f)

Figure 10a-10f: Equilibrium structures of NICPIC - Front view without hydrogen bonding (a), front view with hydrogen bonding (b), top view without hydrogen bonding (c), top view with hydrogen bonding (d), side view without hydrogen bonding (e), side view with hydrogen bonding (f) and hydrogen bonding populations are represented in yellow color.

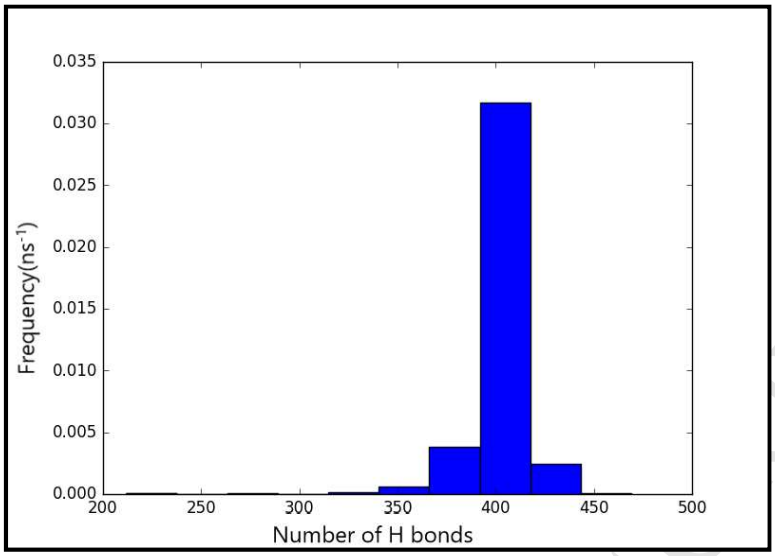

Figure 11: Graph of Frequency (ns^{-1}) versus Number of hydrogen bonds obtained from MD simulation

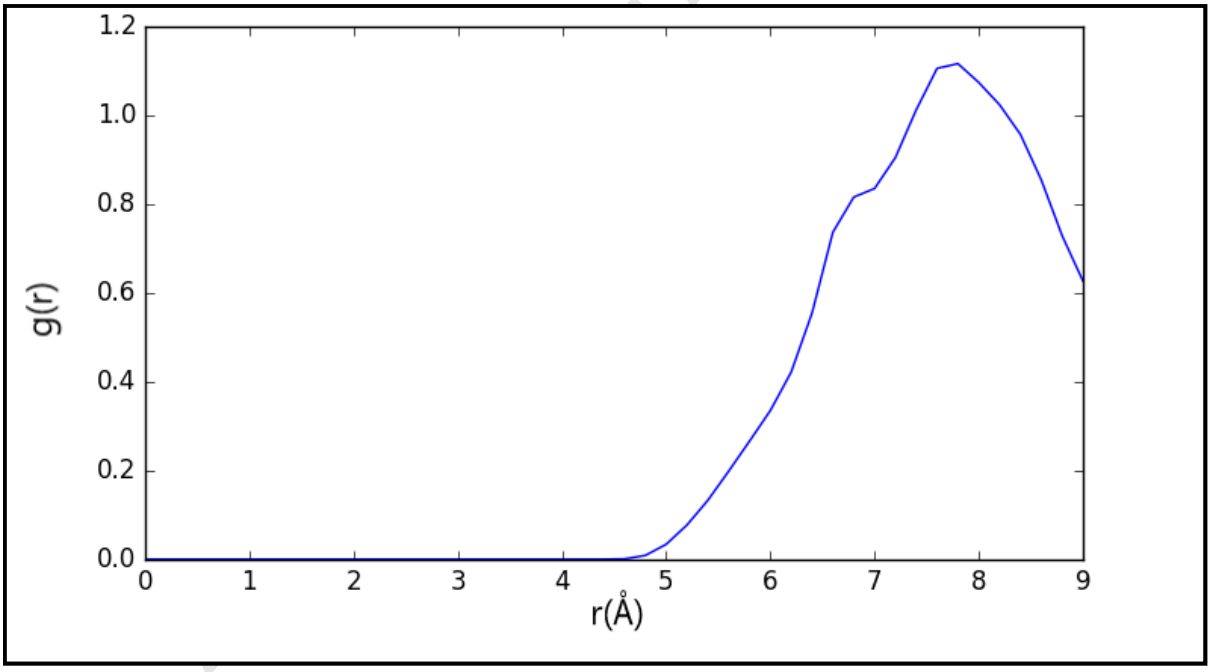

Figure 12: RDF spectrum of NICPIC

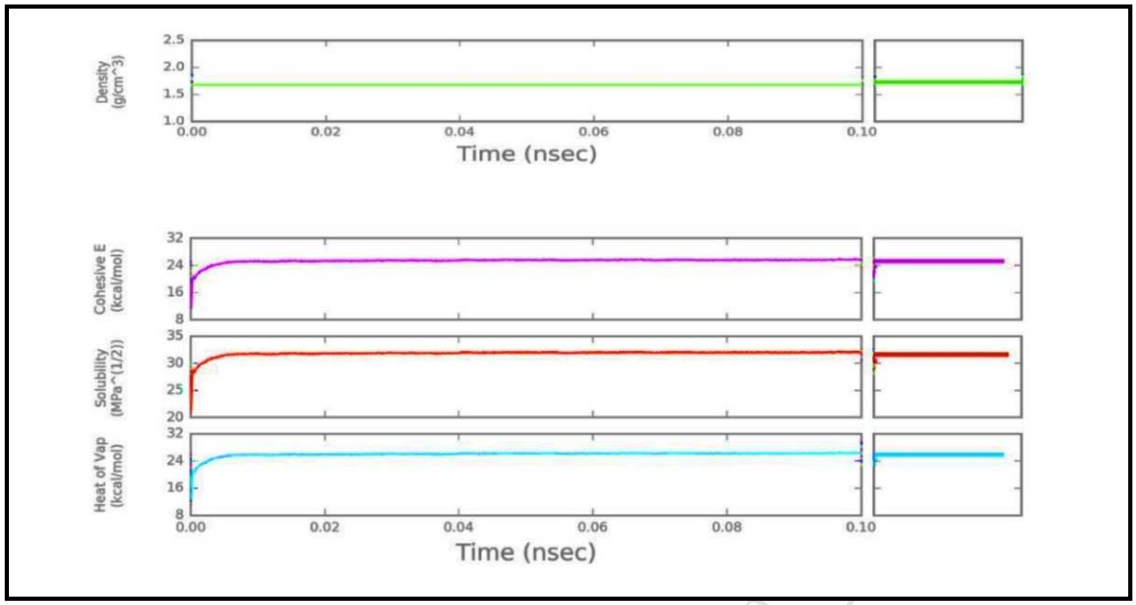

Figure 13: Graphical representation of bulk properties simulation for NICPIC

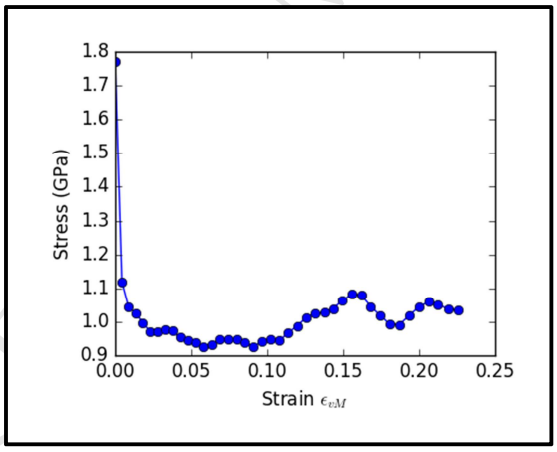

Figure 14: Simulated stress-strain curve for NICPIC

Do Hydrogen Bonding and Noncovalent Interactions Stabilize Nicotinamide-Picric Acid Cocrystal Supramolecular Assembly?

U. Likhitha[a], B. Narayana[a b]*, B. K. Sarojini[a], Anupam. G. Lobo[c], Gopal Sharma[d], Surbhi Pathania[d], Rajni Kant[d]

[a]Department of Industrial Chemistry, Mangalore University, Mangalagangothri-574199, India

[b]Department of Studies in Chemistry, Mangalore University, Mangalagangothri-574199, India

[c]School of Chemical Sciences, Mahatma Gandhi University, Kottayam -686560, India.

[d]Department of Physics, University of Jammu, Jammu Tawi - 180 006, India.

Highlights

- Stabilization of molecular cocrystal of nicotinamide with picric acid by noncovalent interactions.
- Cocrystal crystalized in the orthorhombic *Pbca* system and refined to R=0.0723 for 1755 observed reflections.
- Molecular dynamic simulations quantified supramolecular architecture of cocrystal.
- Simulation could be used to predict the types of hydrogen bonds present in the system.